Supplementary Materials for

Photochemical [2+2] reaction-tuned spin-crossover cooperativity in an Fe(II)-Ag(I) bimetallic Hofmann-type framework

Long-Fei Wang,[1] Liang Wu,[1] Guo-Zhang Huang,[2] Si-Guo Wu[2*] & Ming-Liang Tong[2]*

CONTENTS

Table S1. Crystallographic data for **1** at 160 K, 120 K and 80 K.

Parameter	**1**		
***T* [K]**	160	120	80
Formula	$C_{30}H_{22}Ag_2FeN_6$		
M_r	738.13		
Crystal system	monoclinic		
Space group	*C*2/*c*		
Wavelength [Å]	0.71073		
***a* [Å]**	15.3710(8)	15.3288(9)	15.2967(9)
***b* [Å]**	14.7255(8)	14.5314(8)	14.2856(8)
***c* [Å]**	14.2686(7)	14.1208(7)	13.9432(7)
***α* [°]**	90	90	90
***β* [°]**	118.523(2)	117.774(2)	116.607(2)
***γ* [°]**	90	90	90
***V* [Å^3]**	2837.6(3)	2783.0(3)	2724.2(3)
Z	4	4	4
ρ_{calcd} **[g cm^{-3}]**	1.728	1.762	1.800
μ **(Mo Kα) [mm^{-1}]**	1.901	1.938	1.980
Refl. coll. / unique	20014 / 3257	15797 / 2619	18983 / 3141
R_{int}	0.0358	0.0390	0.0806
R_1 **[$I > 2\sigma(I)$]**[a]	0.0214	0.0463	0.0273
wR_2 **[all data]**[b]	0.0487	0.0947	0.0576
Goof on F^2	1.040	1.148	1.040

[a] $R_1 = \sum||F_o| - |F_c||/\sum|F_o|$, [b] $wR_2 = [\sum w(F_o^2 - F_c^2)^2/w(F_o^2)^2]^{1/2}$.

Table S2. Crystallographic data for **2** at 220 K, 123 K, and 80 K.

Parameter	**2**		
***T* [K]**	220	123	80
Formula	$C_{30}H_{22}Ag_2FeN_6$		
M_r	738.13		
Crystal system	monoclinic		
Space group	*C*2/*c*		
Wavelength [Å]	0.71073		
***a* [Å]**	15.7872(16)	15.6411(18)	15.554(2)
***b* [Å]**	14.1947(16)	14.0881(18)	13.941(2)
***c* [Å]**	14.8973(18)	14.7077(16)	14.5552(17)
***α* [°]**	90	90	90
***β* [°]**	118.432(5)	118.026(4)	117.344(5)
***γ* [°]**	90	90	90
***V* [Å^3]**	2935.7(6)	2860.8(6)	2803.3(6)
Z	4	4	4
ρ_{calcd} **[g cm^{-3}]**	1.670	1.714	1.749
μ **(Mo Kα) [mm^{-1}]**	1.838	1.886	1.924
Refl. coll. / unique	28434 / 3443	28687 / 3369	27896 / 3266
R_{int}	0.1412	0.1078	0.1372
R_1 **[$I > 2\sigma(I)$]**[a]	0.0740	0.0542	0.0520
wR_2 **[all data]**[b]	0.1264	0.1142	0.1008
Goof on F^2	1.070	1.059	1.030

[a] $R_1 = \sum||F_o| - |F_c||/\sum|F_o|$, [b] $wR_2 = [\sum w(F_o^2 - F_c^2)^2/w(F_o^2)^2]^{1/2}$.

Table S3. Selected structural parameters for **1** and **2**.

Parameter	1			2		
***T* [K]**	160	120	80	220	123	80
<Fe1–N1>[a] [Å]	2.1475(15)	2.037(5)	1.944(2)	2.14(2) 2.13(2)	2.067(19) 2.050(19)	2.00(3) 1.99(3)
<Fe1–N2>[a] [Å]	2.1560(15)	2.055(5)	1.942(2)	2.12(2) 2.17(2)	2.075(17) 2.076(18)	2.02(2) 1.97(2)
<Fe1–N3>[a] [Å]	2.2206(15)	2.122(4)	2.018(2)	2.211(10) 2.209(10)	2.130(9) 2.112(8)	2.043(10) 2.065(10)
<Fe1–N>[b] [Å]	2.1747(15)	2.0713(5)	1.968(2)	2.163(10)	2.085(19)	2.015(10)
ΣFe1[c] [°]	16.66(6)	12.08(17)	12.64(8)	13.809(12)	12.836(702)	12.559(682)
Fe1-N1≡C1[d] [°]	163.93(15)	166.6(4)	170.54(19)	170(3) 175.74(24)	168.7(17) 175.764(20)	172(2) 177.869(27)
Fe1-N2≡C2[d] [°]	169.65(15)	171.9(5)	174.6(2)	170.8(19) 165.09(26)	171.4(11) 169.096(17)	173.6(13) 172.467(19)
Fe1-N≡C[e] [°]	166.79(15)	169.25(5)	172.57(19)	170.41(26)	171.24(16)	173.98(15)
C1-Ag1-C2[f] [°]	170.09(8)	170.2(2)	170.19(9)	164.8(12) 173.8(15)	162.7(9) 175.1(8)	165.0(10) 174.5(9)
Ag1-C1≡N1[g] [°]	172.38(18)	171.8(5)	170.2(2)	169(3) 166(3)	169(3) 168(2)	172(3) 168(3)
Ag1-C2≡N2[h] [°]	172.12(17)	171.3(5)	170.7(2)	174(4) 172(4)	175.9(18) 173.0(13)	174.5(15) 168.7(15)
Fe···Fe[i] [Å]	14.2686(7)	14.1208(7)	13.9432(7)	13.8548(82)	13.7419(62)	13.6239(62)
Fe···Fe[j] [Å]	7.5895(4)	7.6263(4)	7.7032(4)	7.8691(86)	7.8306(63)	7.8457(70)

[a]The Fe–N bond lengths (Å); [b] The average Fe–N bond lengths; [c]Octahedral distortion parameters (°); [d] Fe–N≡C angles (°) within Hofmann layer; [e] Average Fe–N≡C angles (°) within Hofmann layer; [f] C–Ag–C angles (°) of $Ag(CN)_2^-$ unit; [g] Ag–C≡N angles (°) of $Ag(CN)_2^-$ unit; [h] Average Fe–N≡C angles (°) within Hofmann layer; [i]The shortest intralayer Fe···Fe distance (Å); [j]The shortest Fe···Fe distance (Å) between the neighboring Hofmann layers.

Table S4. Geometrical parameters of offset face-to-face π···π interactions between the aromatic rings of 3-spy ligands in **1** and *rtcc*-hh substituted cyclobutanes in **2** at different temperatures.

Parameter	**1**			**2**		
***T* [K]**	160	120	80	220	123	80
***Z*[a] [Å]**	3.63 / 3.92	3.61 / 3.95	3.61 / 3.98	3.77	3.73	3.70
***β*[b] [°]**	3.78 / 3.24	3.86 / 4.93	3.77 / 7.12	0	0	0
***d*[c] [Å]**	3.55 / 3.77	3.51 / 3.77	3.48 / 3.75	3.31	3.29	3.23
***r*[d] [Å]**	0.76 / 1.07	0.84 / 1.18	0.96 / 1.33	1.80	1.76	1.80

[a]The *Z* parameter represents the distance (Å) between the centers of aromatic rings; [b]The *β* parameter represents the dihedral angle (°) between the measured aromatic rings; [c]The *d* parameter represents the distance (Å) between the center of an aromatic ring and the plane of another aromatic ring; [d]The *r* parameter represents the offset distance (Å) between the centers of the aromatic rings, which is obtained from the equation $\sqrt[2]{Z^2 - d^2}$.

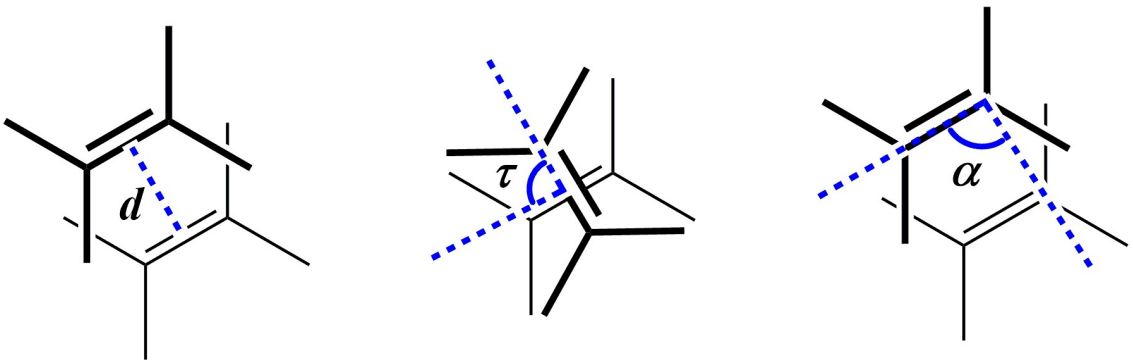

Scheme S1. Geometrical parameters are used to evaluate the potential for photoreactivity. The ***d*** parameter represents the distance (Å) between the double bonds. The τ parameter provides an angular indication of how close the double bonds are to being parallel and the α parameter is referred to the slip angle.

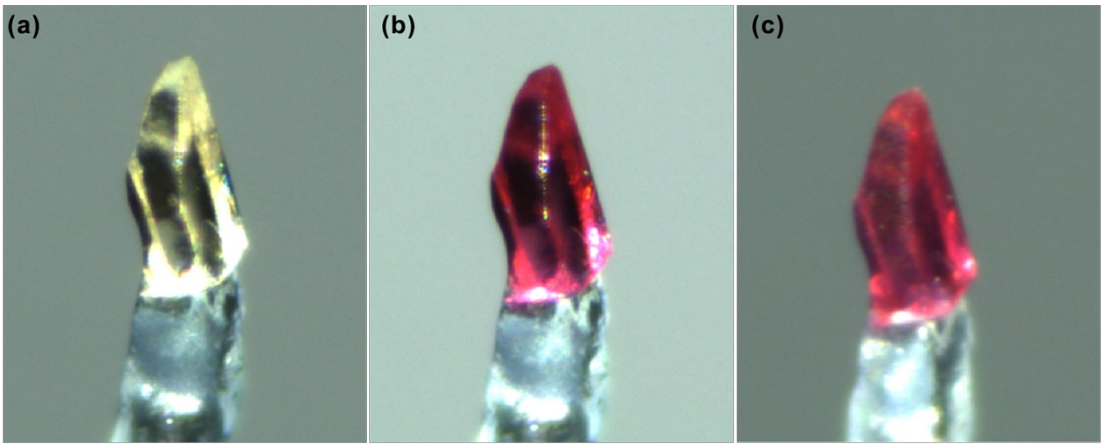

Figure S1. A view showing the single crystal for 1 under 160 K (a), 120 K (b), and 80 K after 5 hours' annealing (c), showing obvious color changes from yellow to red due to SCO behavior.

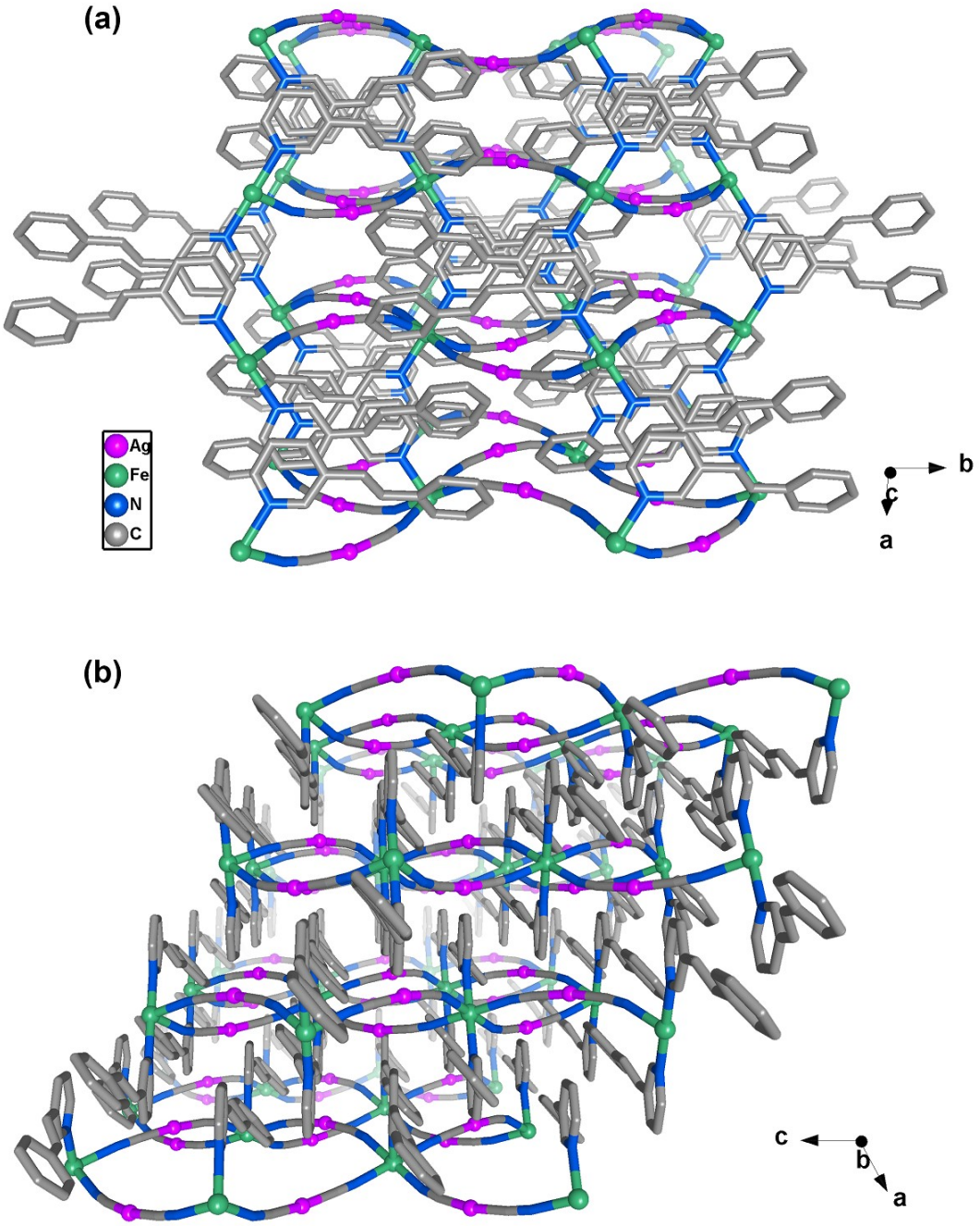

Figure S2. A view showing the packing arrangement of the 2D $[Fe(3\text{-spy})_2\{Ag(CN)_2\}_2]$ layer in **1** along the *c* (a) and *b* (b) axis. For clarity, the H atoms are omitted.

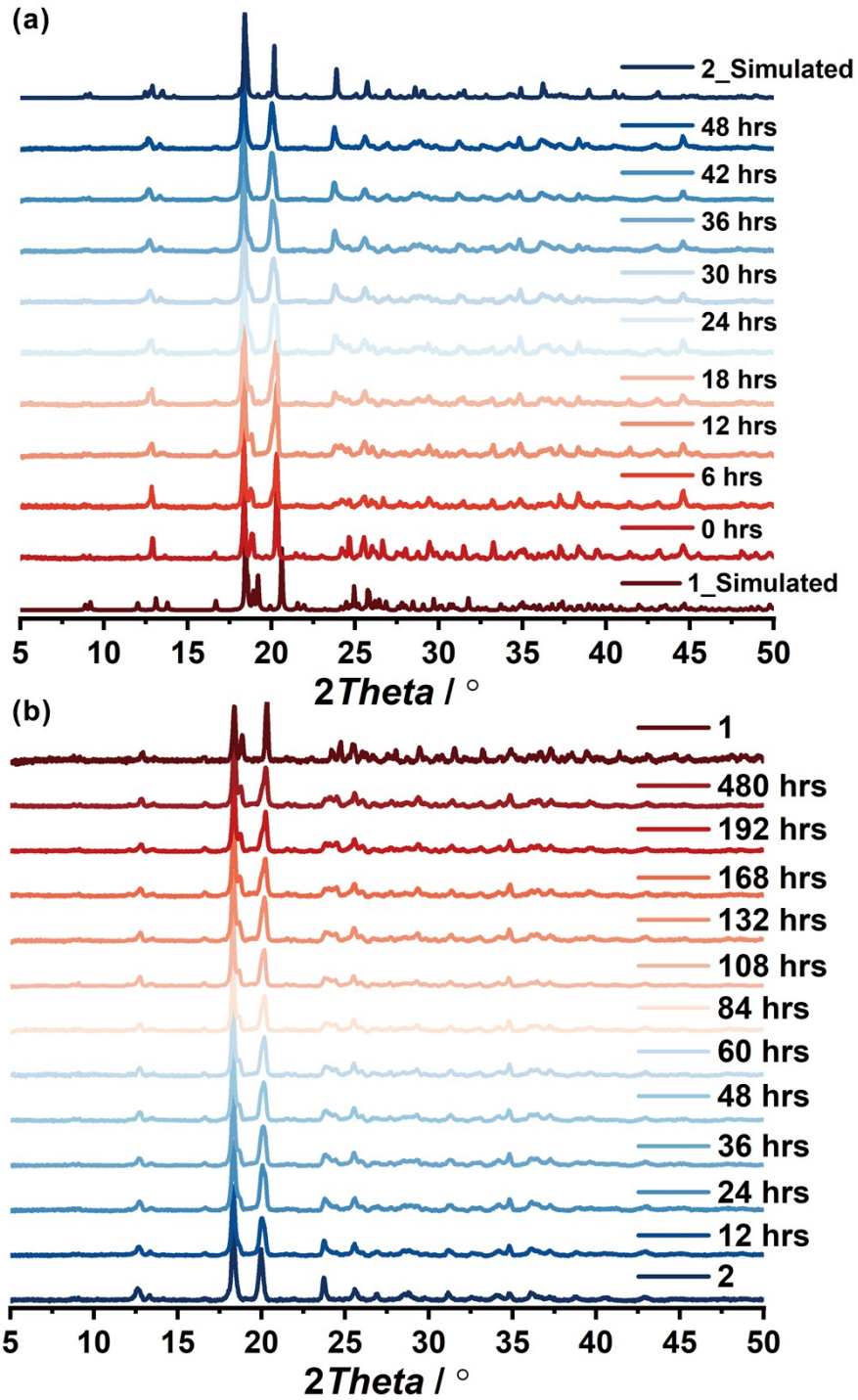

Figure S3. (a) The Powder X-ray diffraction patterns of complex **1** at different 365nm UV light irradiation time; (b) The Powder X-ray diffraction patterns of complex **2** at different 254 nm UV light irradiation time.

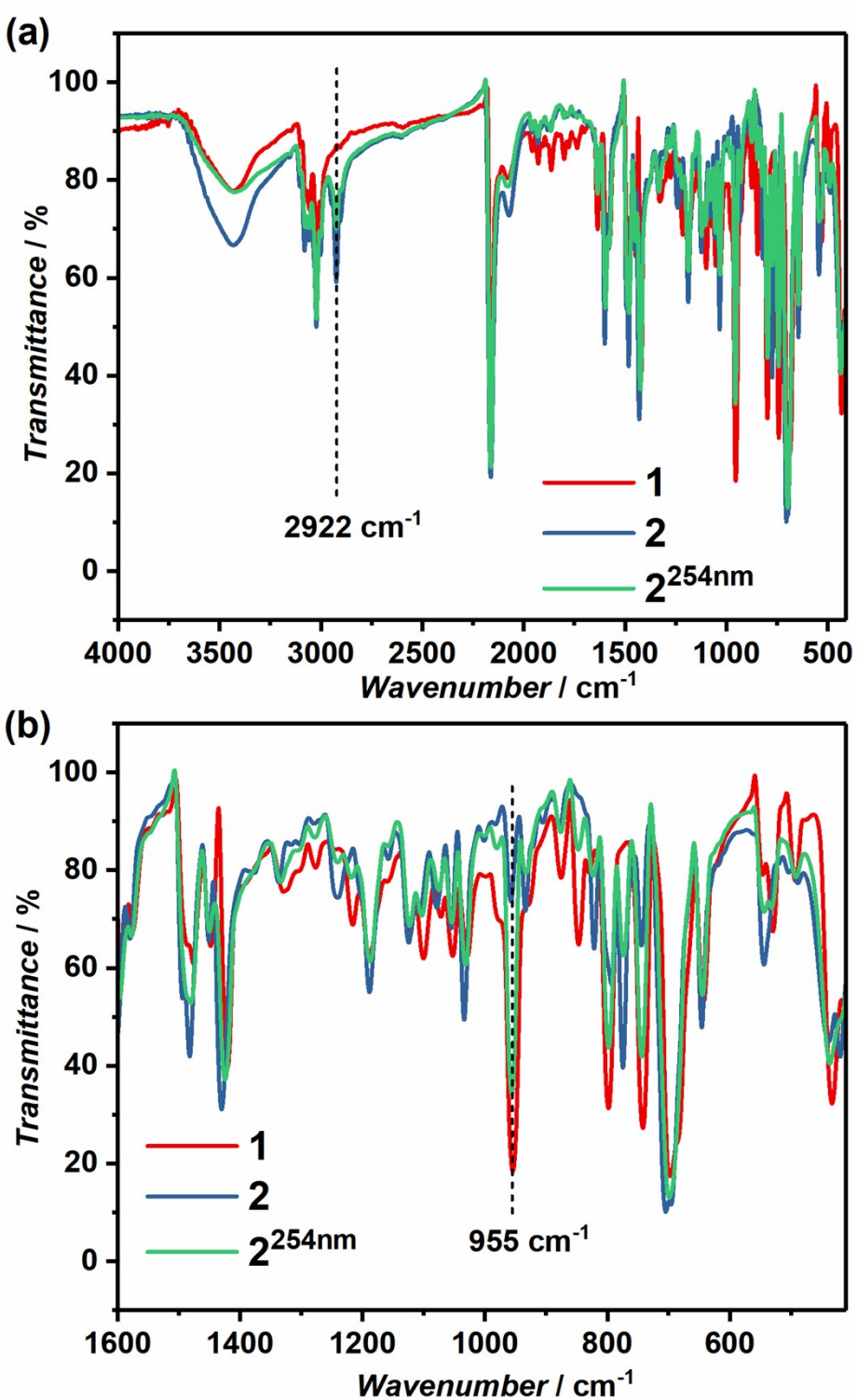

Figure S4. The IR spectra show the variation of the saturated C-H stretching vibrations at 2922 cm^{-1} (a) and the C=C-H out-of-plane bending vibrations at 955 cm^{-1} (b) for **1**, **2**, and $\mathbf{2}^{\mathbf{254nm}}$.

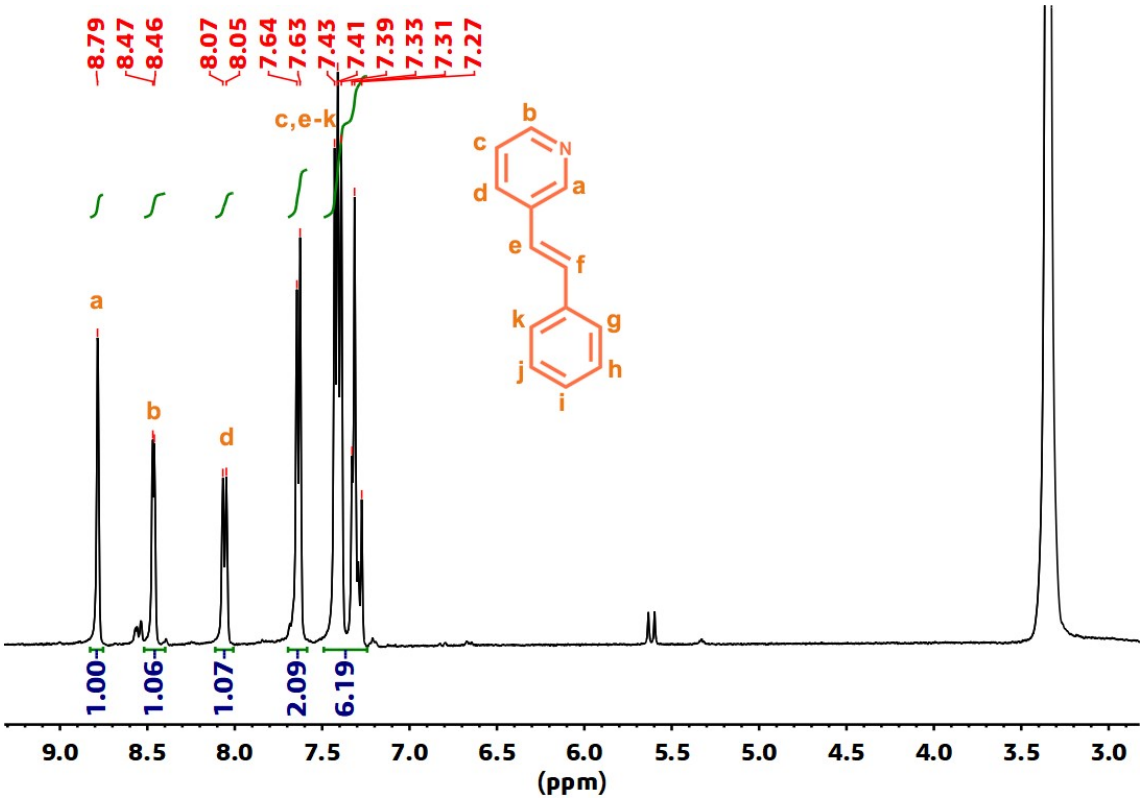

Figure S5. ^{1}H NMR spectra of the framework digestion products of **1**.

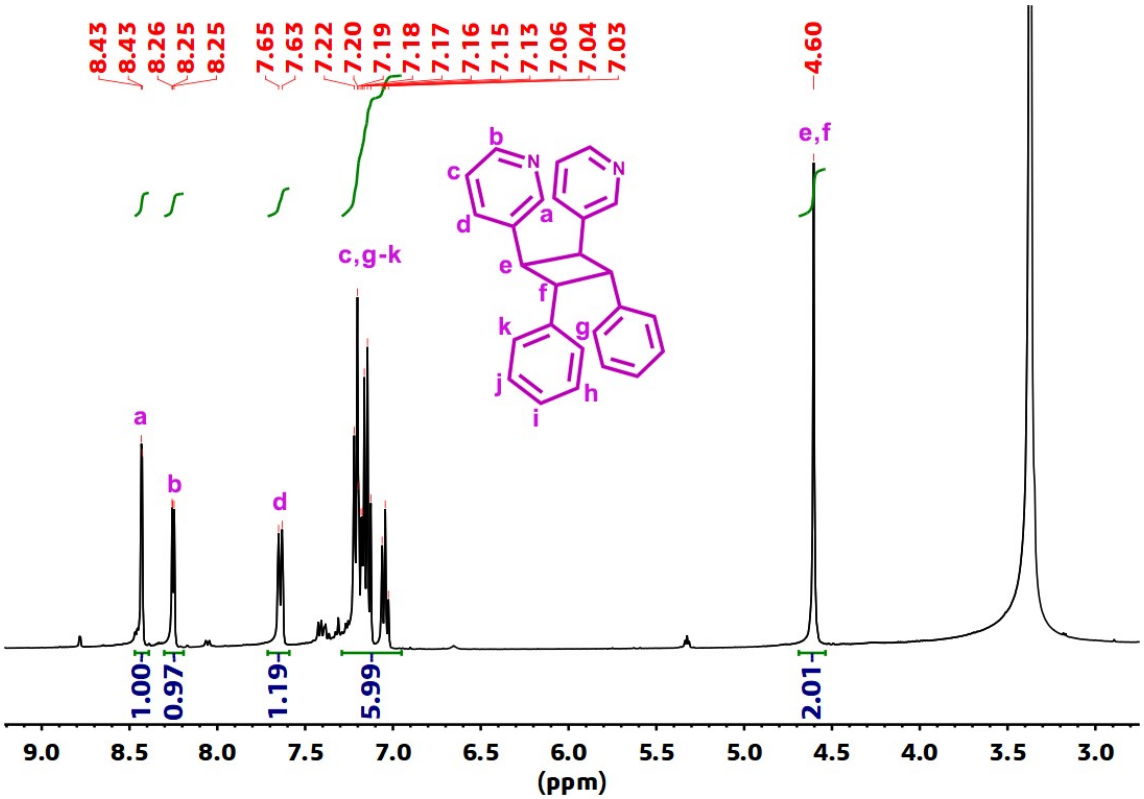

Figure S6. ^{1}H NMR spectra of the framework digestion products of **1** after 365 nm UV irradiation for 48 hours.

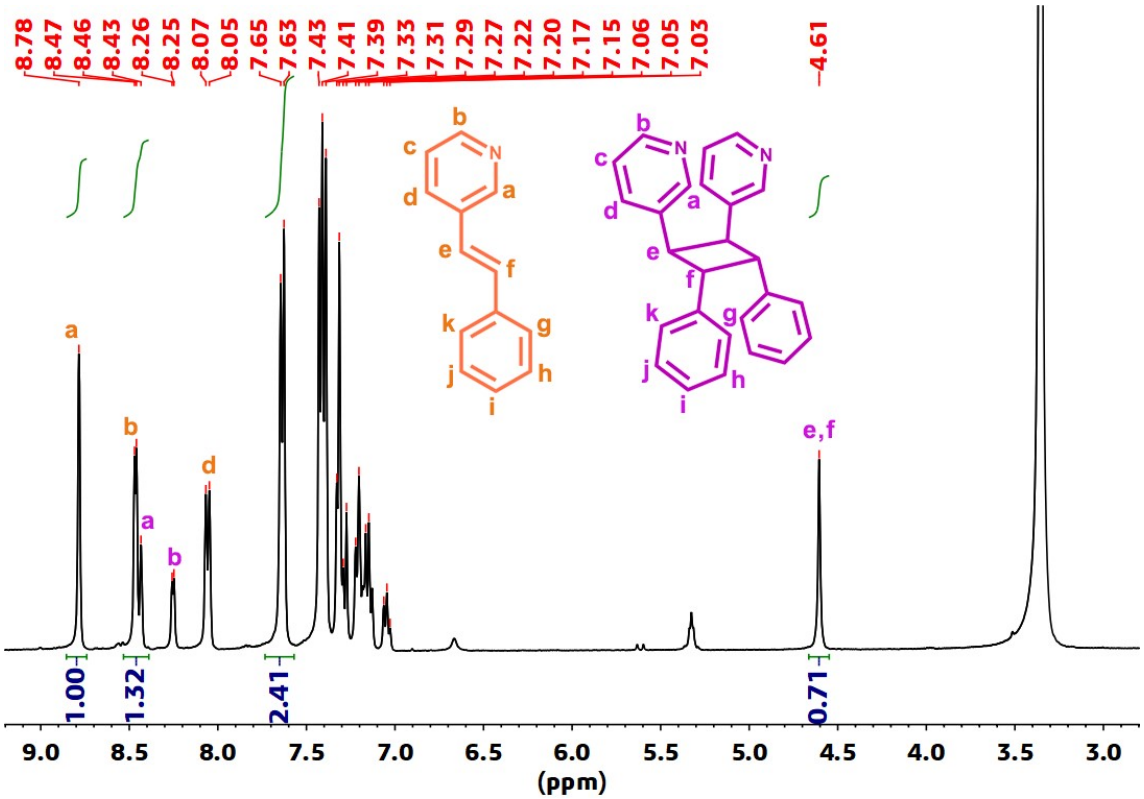

Figure S7. ^{1}H NMR spectra of the framework digestion products of **1** after 365 nm UV irradiation for 3 hours.

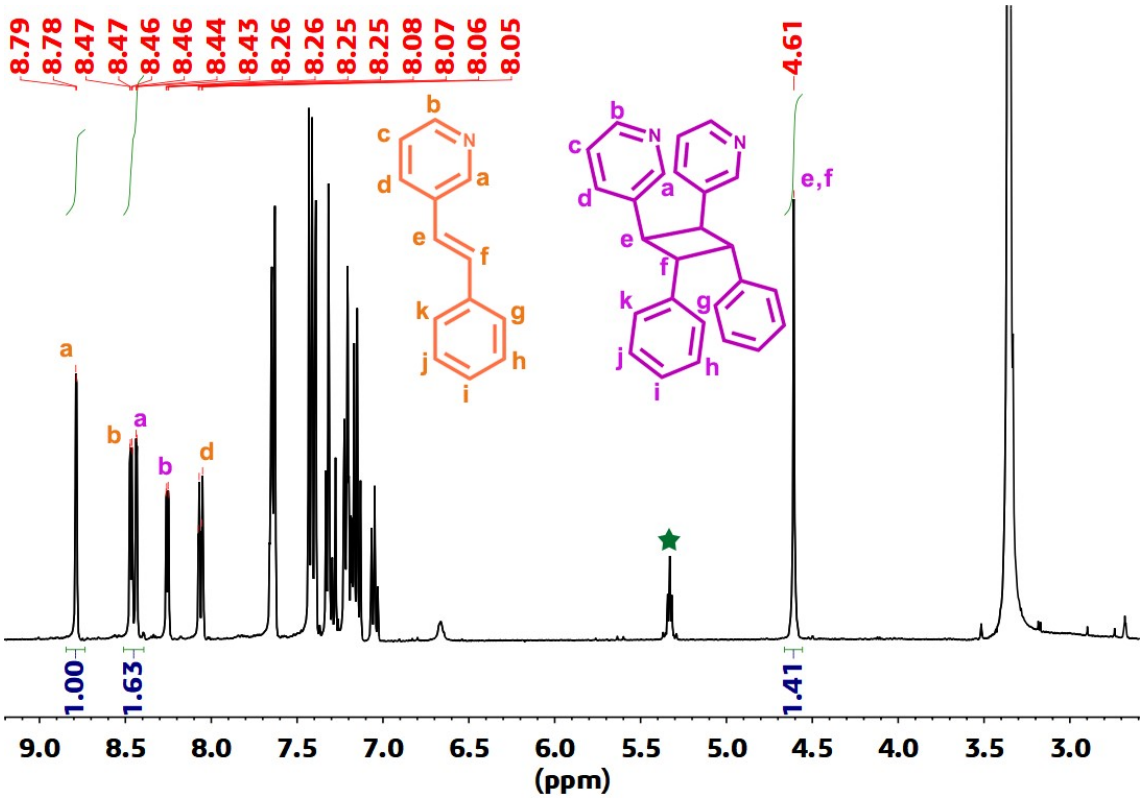

Figure S8. ^{1}H NMR spectra of the framework digestion products of **1** after 365 nm UV irradiation for 12 hours.

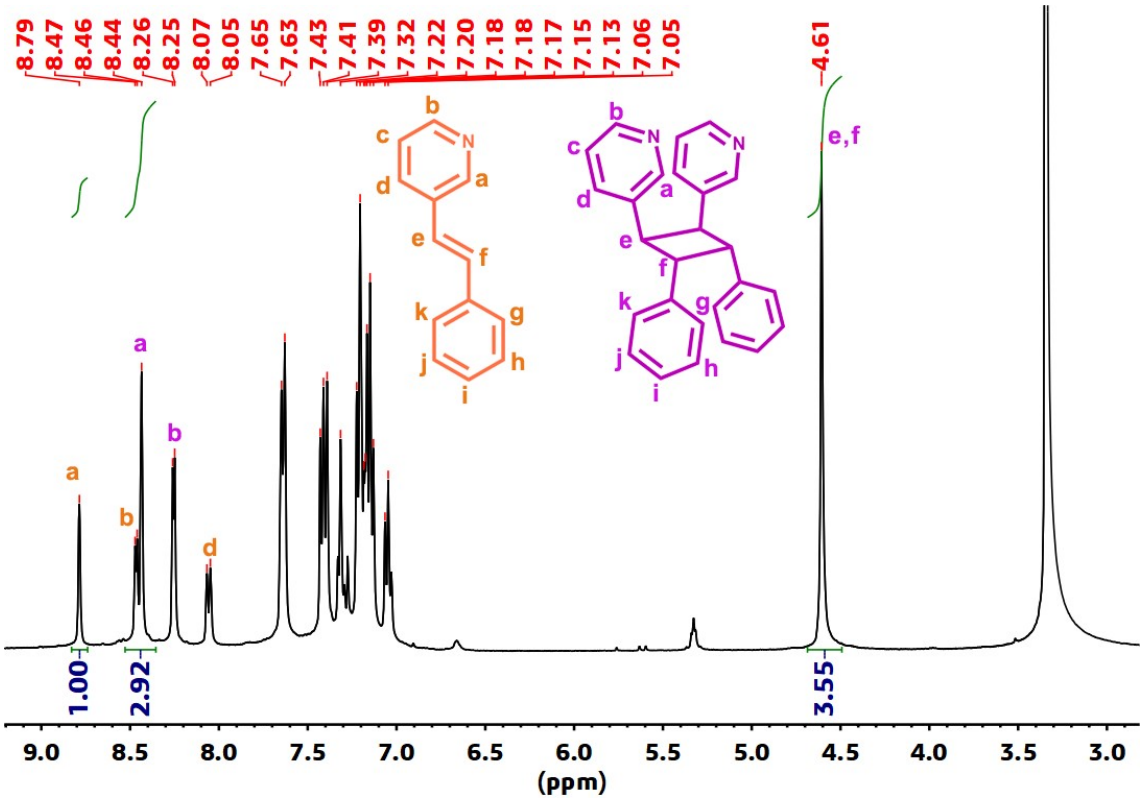

Figure S9. ^{1}H NMR spectra of the framework digestion products of **1** after 365 nm UV irradiation for 24 hours.

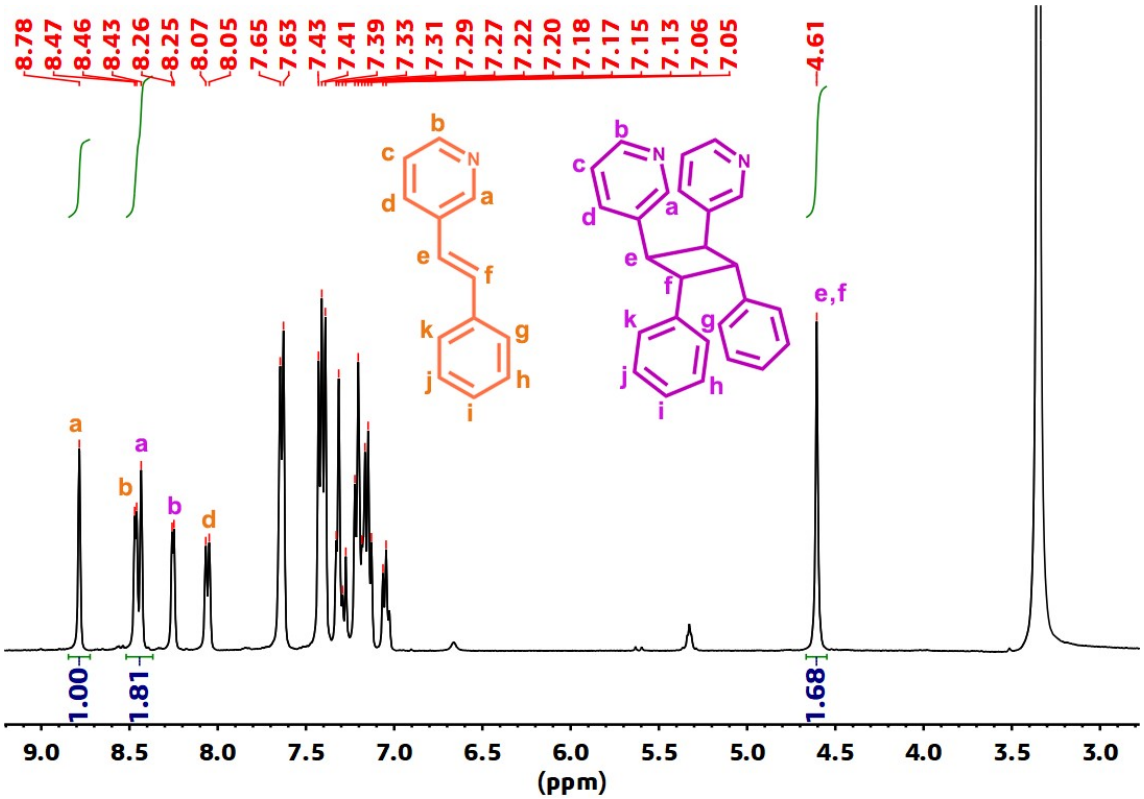

Figure S10. ^{1}H NMR spectra of the framework digestion products of **2** after 254 nm UV irradiation for 20 days.

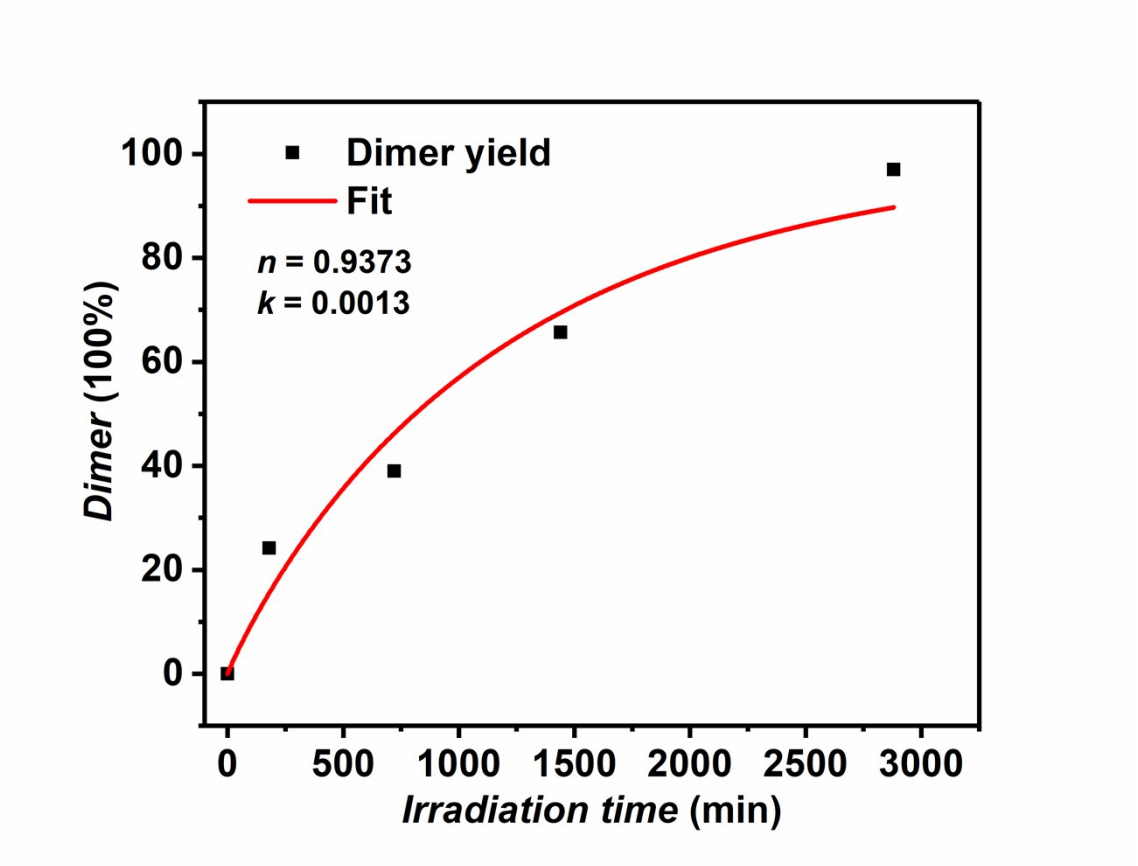

Figure S11. Sharp–Hancock plot of **1** under 365 nm irradiation.

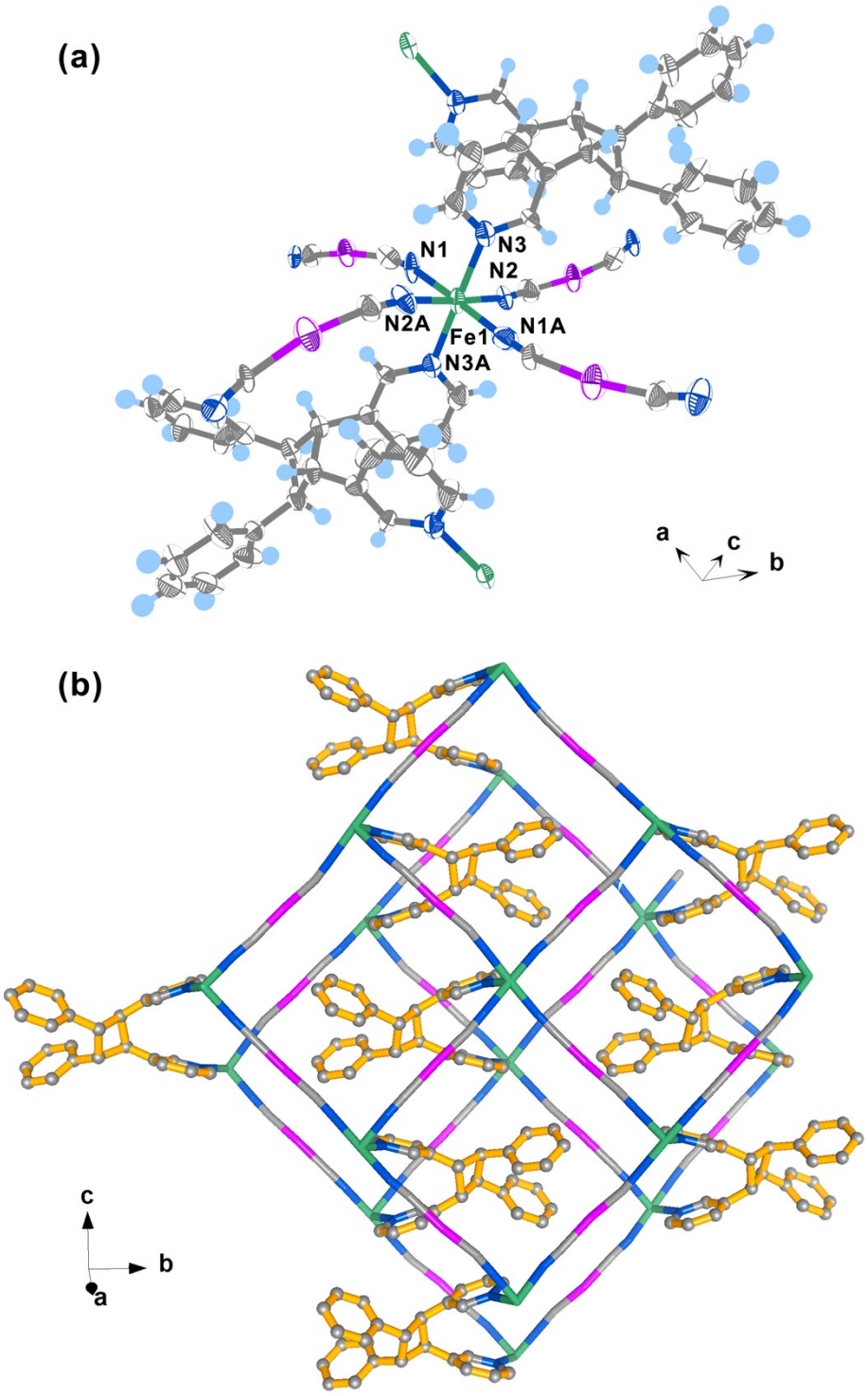

Figure S12. (a) An ORTEP view of the coordination sphere around the Fe(II) center in **2** at 220 K with thermal ellipsoids depicted at 50% probability and the atoms labelled accordingly.; (b) A view of the structure for **2** along the *a* axis. For clarity, the disordered part of the structure and the H atoms are omitted.

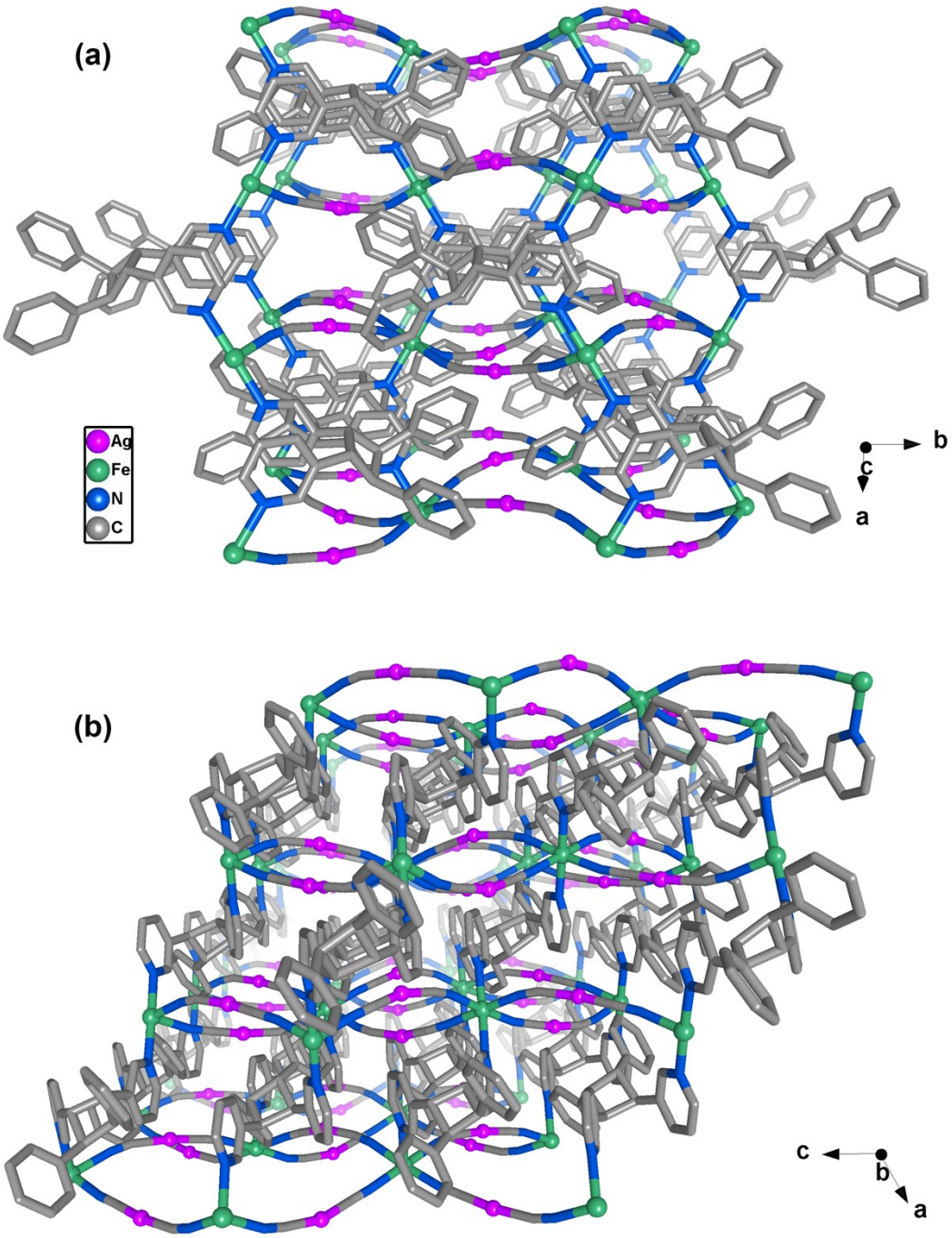

Figure S13. A view of the irradiated structure for **2** along the *c* (a) and *b* (b) axis. For clarity, the disordered part of the structure and the H atoms are omitted.

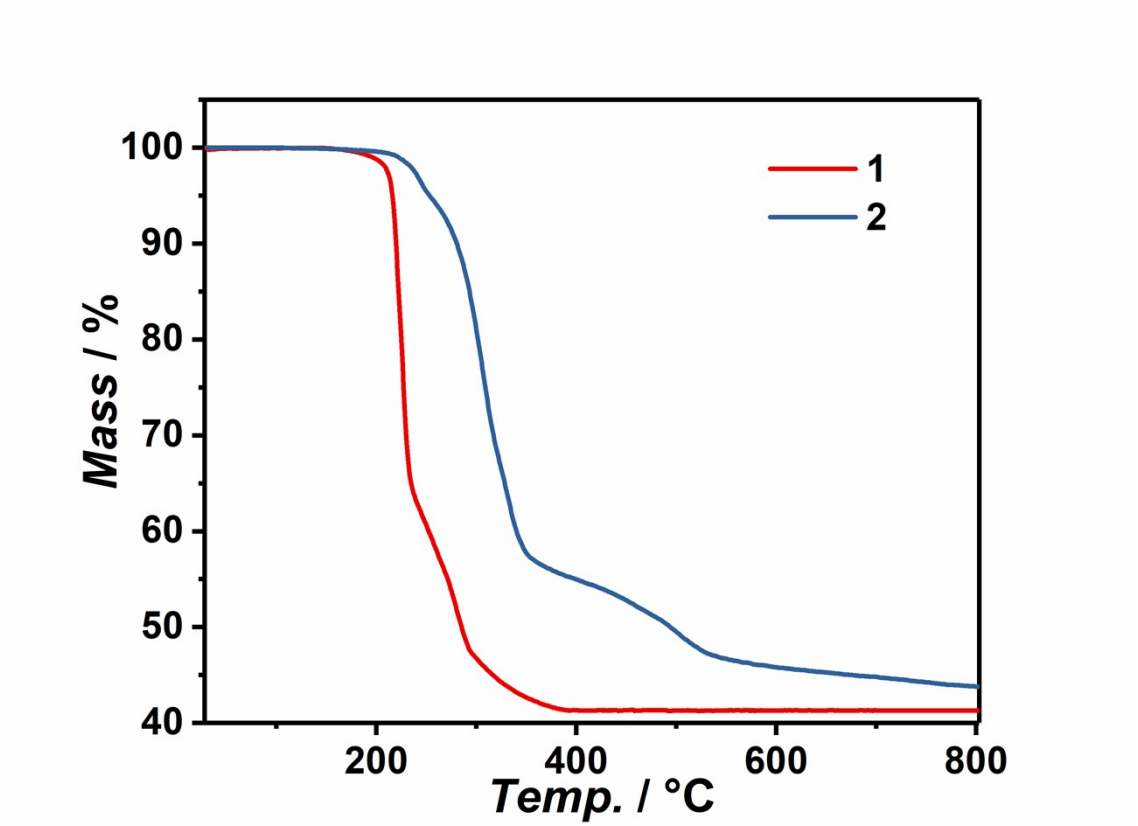

Figure S14. Thermogravimetric-mass spectroscopy analyses of **1** (red line) and **2** (blue line).

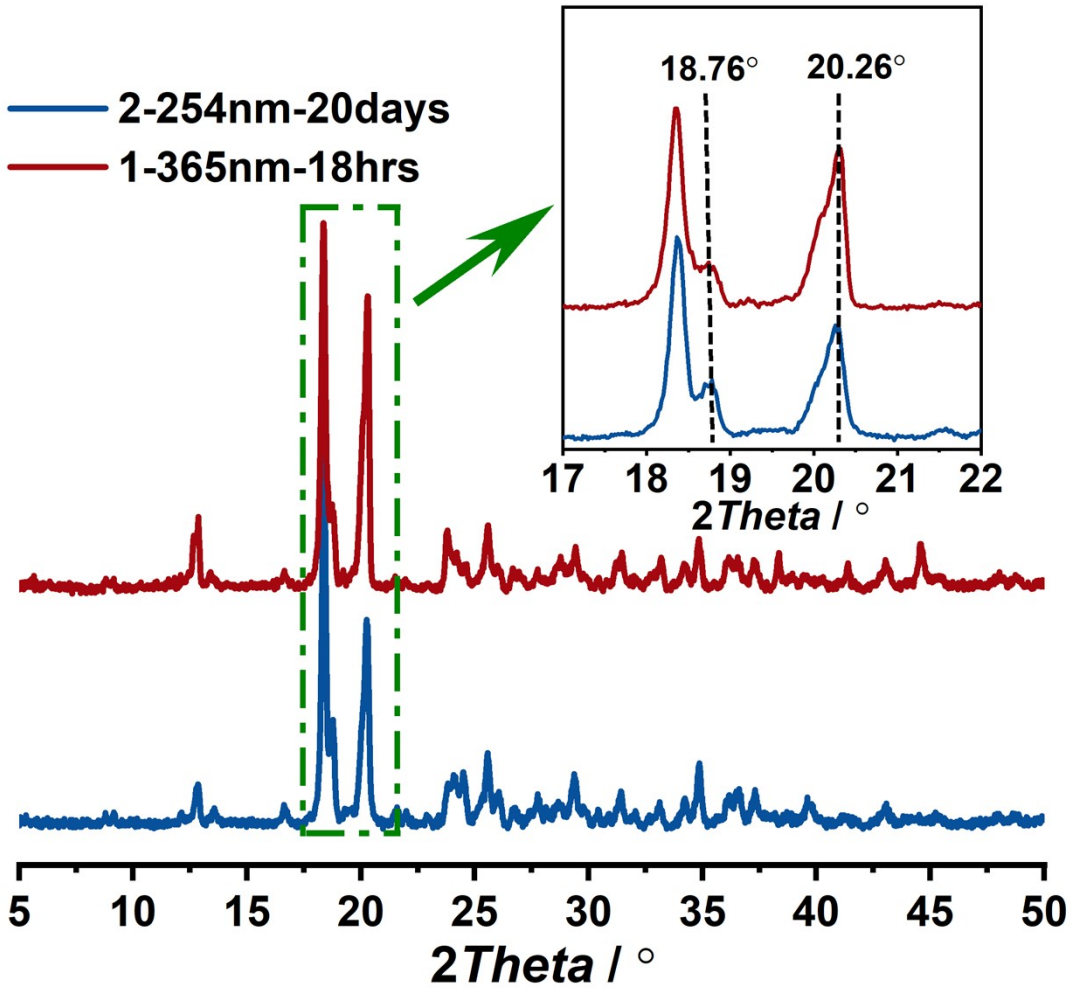

Figure S15. A comparison of powder X-ray diffraction patterns of **2** after 254 nm irradiation for 20 days and **1** after 365 nm irradiation for 18 hours.

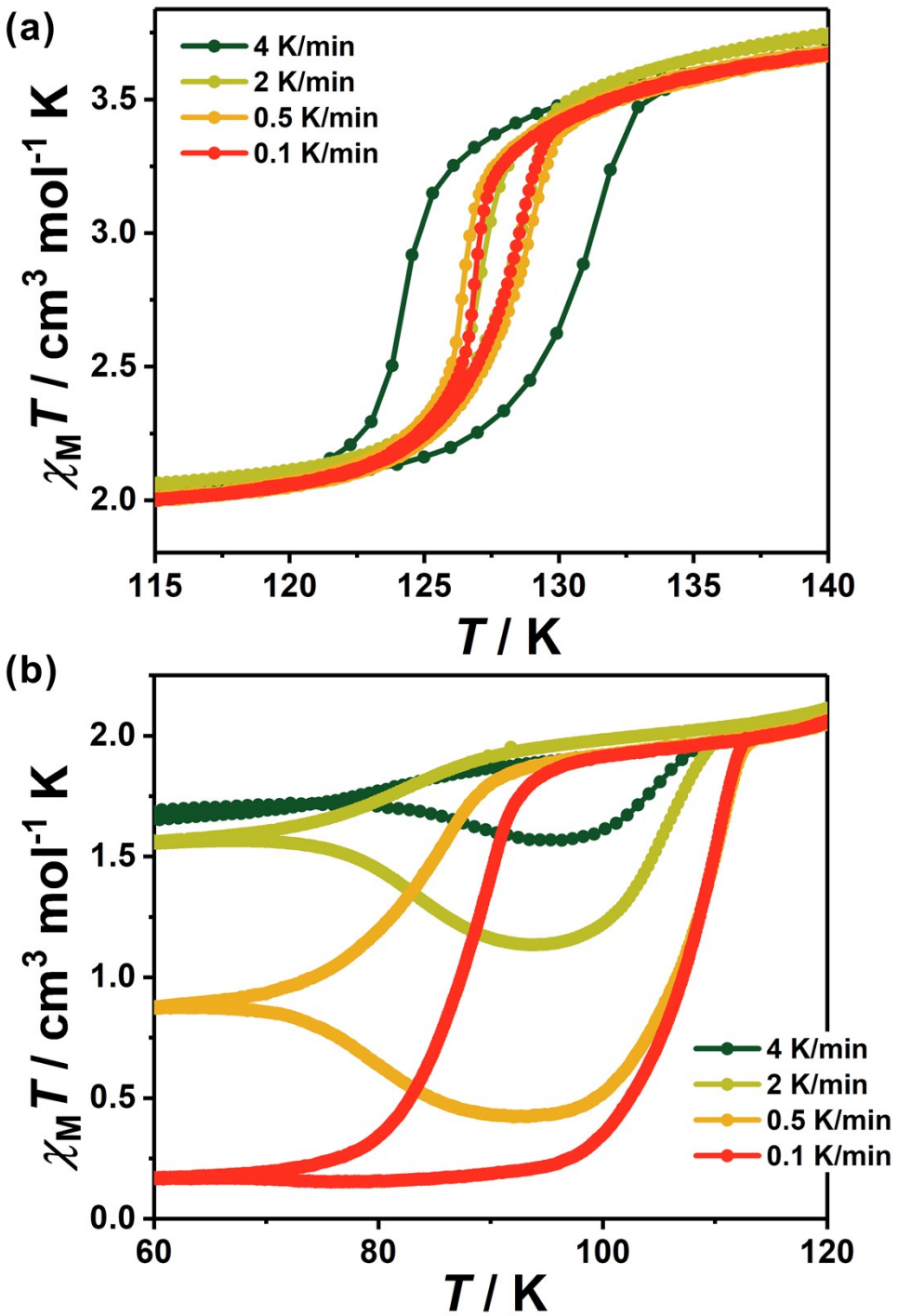

Figure S16. An enlargement of the temperature dependent magnetic susceptibility data for complex **1** at the first (a) and second (b) spin-crossover step under different sweep rate.

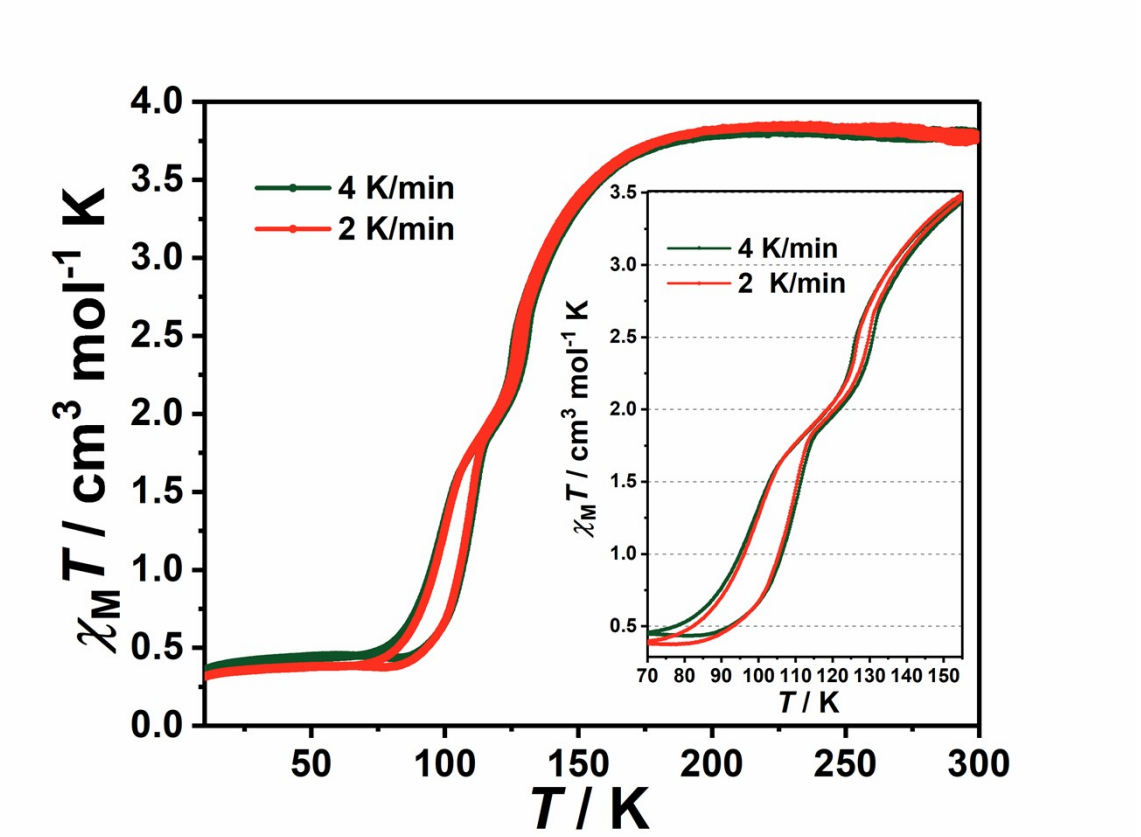

Figure S17. The temperature-dependent molar magnetic susceptibility $\chi_M T$ plot for **1** under 365 nm irradiation for 3 hours. The inset corresponds an enlargement of $\chi_M T$ *vs* T plot in the range of 70–155 K.

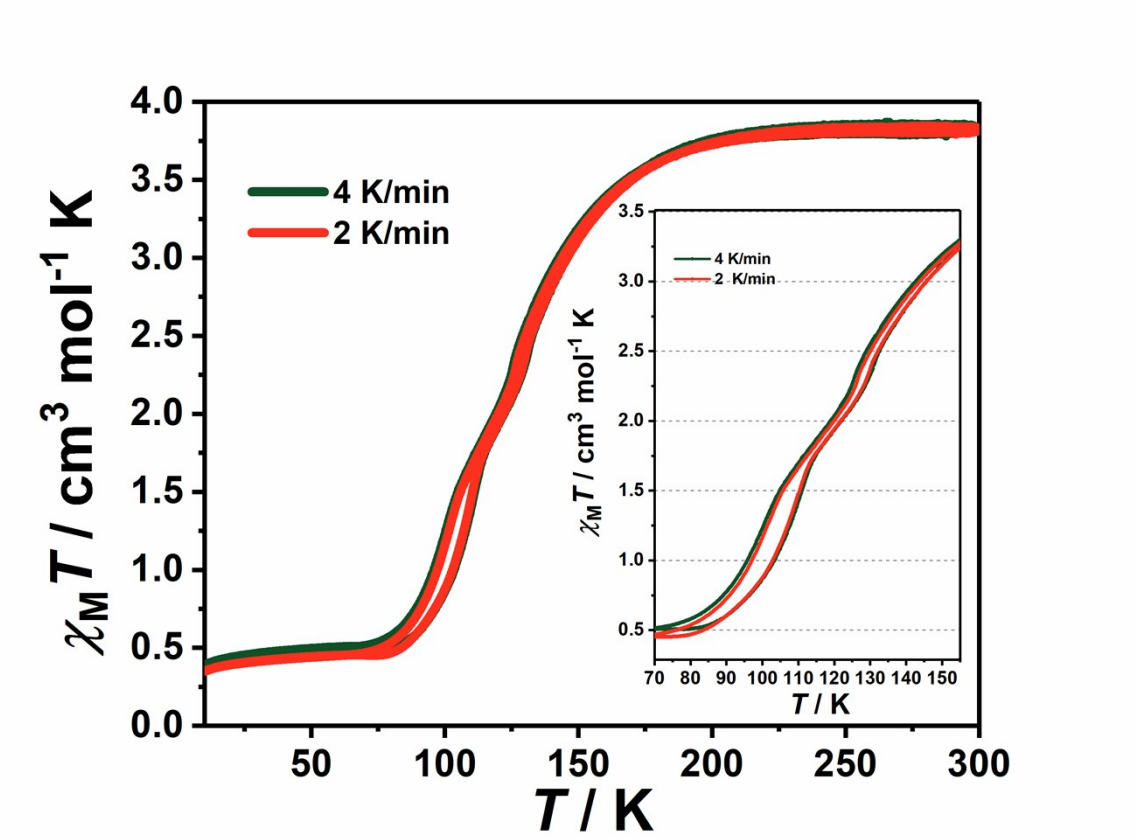

Figure S18. The temperature-dependent molar magnetic susceptibility $\chi_M T$ plot for **1** under 365 nm irradiation for 12 hours. The inset corresponds an enlargement of $\chi_M T$ *vs* T plot in the range of 70–155 K.

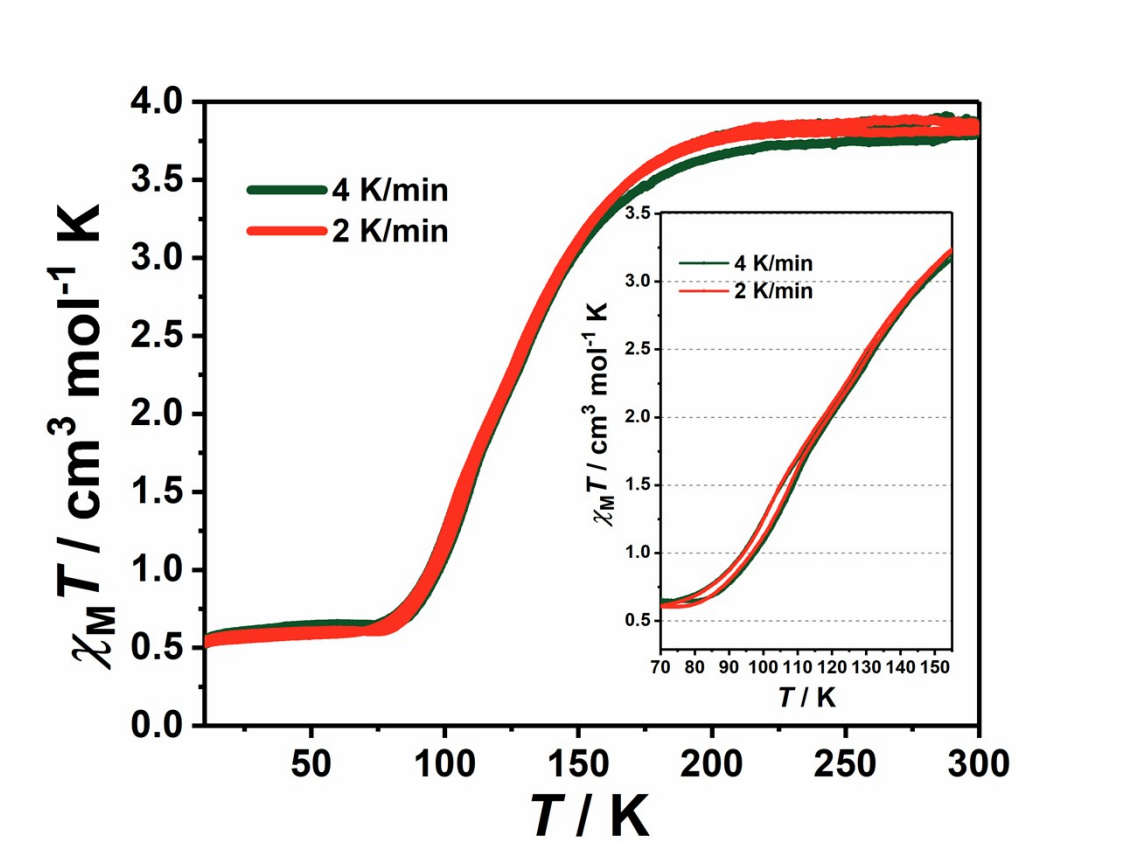

Figure S19. The temperature-dependent molar magnetic susceptibility $\chi_M T$ plot for **1** under 365 nm irradiation for 24 hours. The inset corresponds an enlargement of $\chi_M T$ *vs* T plot in the range of 70–155 K.

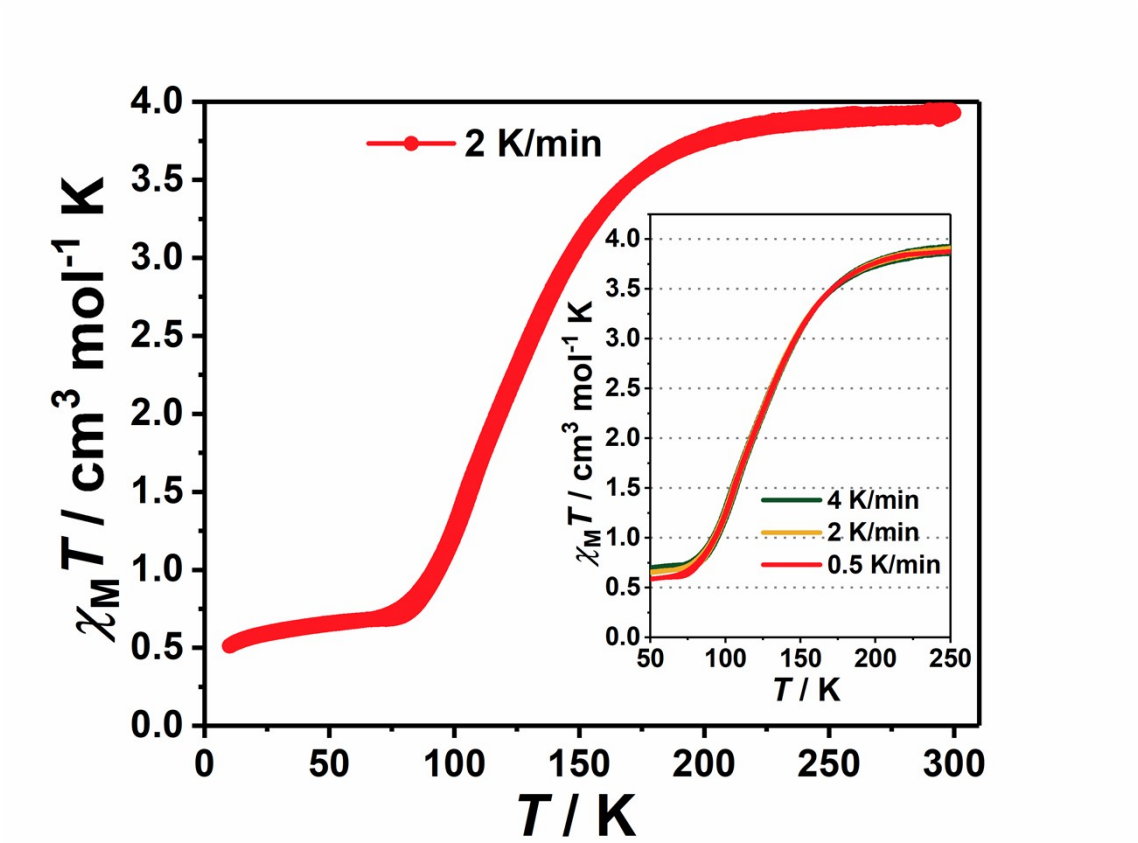

Figure S20. The temperature-dependent molar magnetic susceptibility $\chi_M T$ plot for **1** under 365 nm irradiation for 48 hours (irradiation product **2**). The inset corresponds an enlargement of $\chi_M T$ *vs* T plot in the range of 50–250 K.

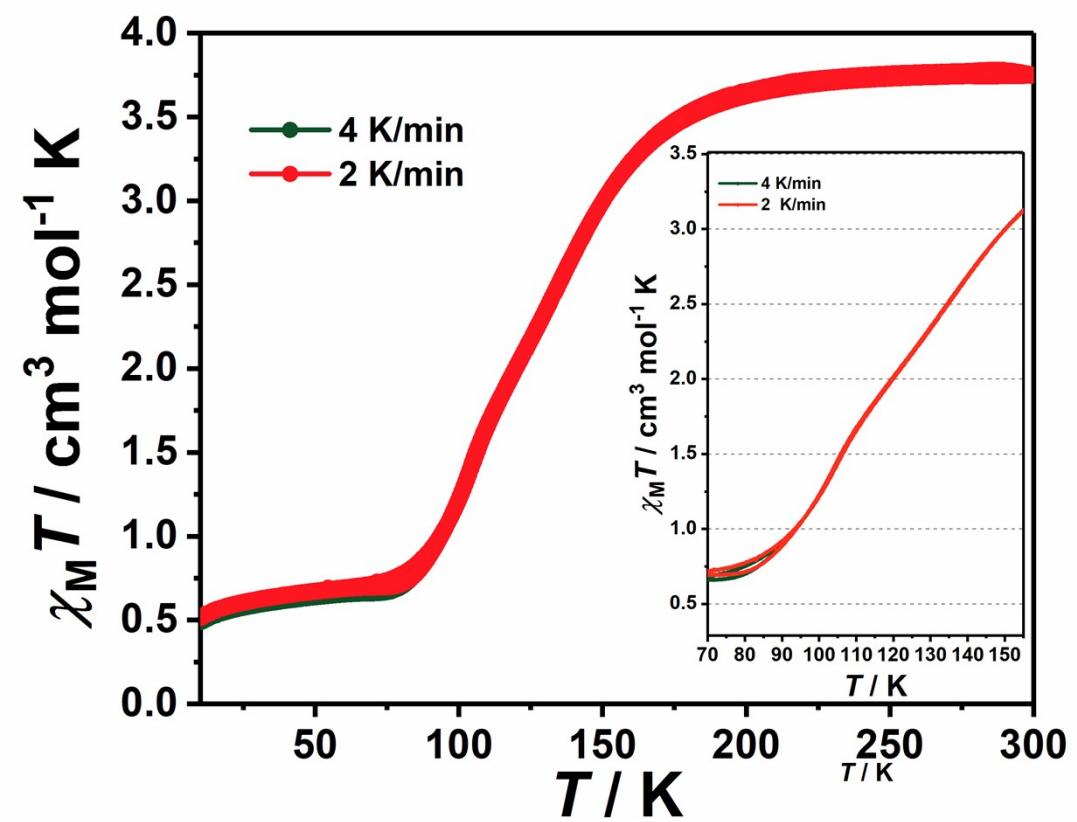

Figure S21. The temperature-dependent molar magnetic susceptibility $\chi_M T$ plot for **2** under 254 nm irradiation for 20 days (irradiation product $\mathbf{2}^{\mathbf{254nm}}$). The inset corresponds an enlargement of $\chi_M T$ *vs* T plot in the range of 70–155 K.

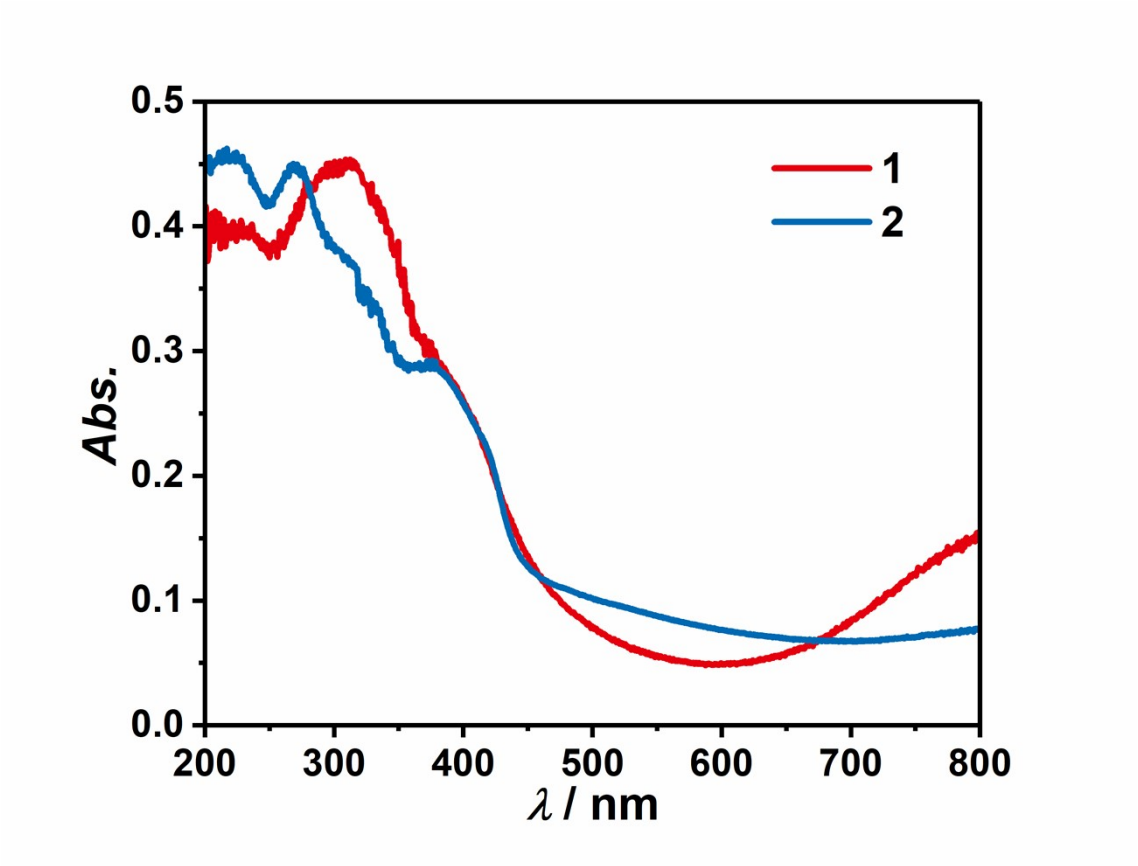

Figure S22. The UV-Vis spectrum for **1** (red line) and **2** (blue line).

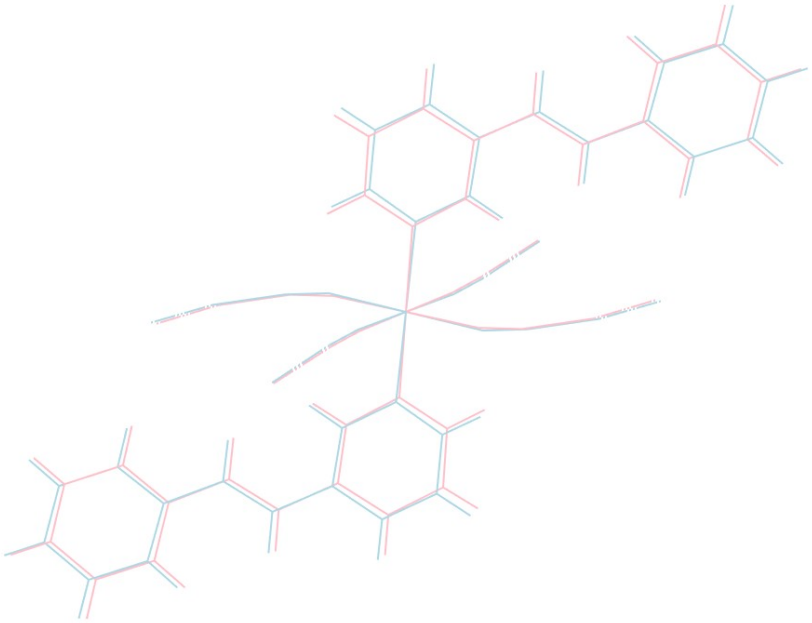

Figure S23. The overlap structures of **1** at 120 K (blue) and 80 K (pink).